Self-consistent Integral Equation Theory for Polyolefins: Comparison to Molecular Dynamics Simulations and X-Ray Scattering

Mathias Pütz[1], John G. Curro[2] and Gary S. Grest[2]

August 7, 2000

[1]Max-Planck-Institut for Polymer Research, Ackermannweg 10, 55128 Mainz, Germany

[2]Sandia National Laboratories, Albuquerque, NM 87185, USA

We report on self-consistent Polymer Reference Interaction Site Model (PRISM) calculations as well as molecular dynamics (MD) simulations for several types of polyolefins. For all polymer types one single set of potential parameters was used. In general we find good semi-quantitative agreement between PRISM and MD results. Further we compare both MD and PRISM results to experimental X-Ray scattering data and show that the potentials used give a good to excellent description of these data. From the quality of the PRISM calculations it is clear that PRISM can be used as an efficient tool in model development.

1 Introduction

Polyolefin polymers represent the largest and most important class of polymers in terms of volume of production. Even though these polymers consist of only single-bonded carbon and hydrogen atoms, they have a wide range of properties that depend sensitively on the molecular architecture. Recent advances in polymer synthesis using metallocene catalysts now give the polymer chemist excellent control over the molecular weight, chain architecture, and stereochemistry of polyolefin macromolecules. In order to guide the synthesis of new polymers with optimized properties, it would be highly desirable if one could compute the effect of polymer architecture on macroscopic properties. In the present investigations we studied the feasability of using theory and simulation for this purpose.

The most accurate approach to modeling polymer melts and blends is through Monte Carlo (MC) or Molecular Dynamics (MD) computer simulations. These simulation methods give formally exact results, but are very computationally demanding, since one needs to treat a relatively large size system consisting of many chains of high molecular weight, at liquid-like densities. An alternative approach is to employ theoretical methods based on integral equation theories of liquids. The theoretical approach is far less demanding from a computational standpoint but, unlike simulations, does not give exact results due to necessary approximations made in order to make the theory computationally tractable. We have previously employed a hybrid of theory and simulation to model polymer melts and blends that is based on the "Polymer Reference Interaction Site Model" or PRISM theory of Curro and Schweizer [1, 2].

In this approach one can map the difficult many chain simulation onto a computationally less demanding single chain simulation. The goal of the present investigation is to test the accuracy of such methods applied to polyolefin models by a direct comparison with full MD simulations.

In previous studies, comparisons were made between PRISM theory and x-ray scattering for polyethylene (PE) [3, 4], isotactic (iPP) and syndiotactic (sPP) polypropylene [5, 6], and polyisobutylene (PIB) [6]. While good agreement was found between theory and experiment for the structure factor, ambiguities exist because of uncertainties in the model parameters and potentials. A more direct test of the theory is to compare with full computer simulation on a multiple chain system at realistic, liquid-like densities. Such a comparison is unambiguous since the same model and potentials are used in both the theory and the simulation. Very good agreement between PRISM theory and simulations was found for coarse grained models consisting of short chain, tangent site polymer melts [7, 8, 9] and blends [10, 11, 12, 13]. Coarse grained representations of polymers are usually adequate for making scaling predictions for long wave length properties on a scale of the radius of gyration. For the purposes of modeling thermodynamic properties that are sensitive to the local packing, however, it is necessary to include the details of the monomeric geometry in a more realistic way. These more realistic models build the monomer structure through multiple, overlapping sites with constrained bond angles and torsional potentials.

Recently, comparisons [14] were made between self-consistent PRISM theory and MD simulations for realistic polyethylene chain melts. Good qualitative agreement between theory and simulation was found, but the theoretical intermolecular pair correlation functions were too soft relative to the simulations for PE. As a consequence, the compressibility predicted by PRISM theory was significantly larger than the simulation values. The inaccuracies in the radial distribution function were likely due to the inability of the theory to handle overlapping sites and local angular correlations between chains. The theoretical predictions for the pair correlation functions were significantly improved by adding a power law tail to the direct correlation function, and choosing the exponent to give the correct compressibility. The purpose of the present investigation is to investigate the accuracy of self-consistent PRISM theory for realistic models of more complex polyolefin melts by directly comparing with full MD simulations. In this work we studied three types of polypropylene: iPP, sPP and head-to-head, syndiotactic propylene denoted as hhPP. In addition we also studied PIB and poly(ethylene) propylene (PEP). The architecture of each is shown in Fig. 1.

We begin with a discussion of the details of the chain models used in both the simulation and theoretical calculations. We then give a brief discussion of PRISM theory where we highlight the method employed in implementing the self-consistent calculation of both the intra and intermolecular structure of the polymer liquids. This is then followed by a discussion of the methods used in the MD simulations. Selected theory and simulation results are then shown and compared for the radial distribution functions, structure factors, dihedral angle distributions and radius of gyrations of the various systems.

2 Models

For the present study we employed a united atom model recently proposed by Martin and Siepmann [15]. This model has been optimized to give correct results for the phase coexistance curve near the liquid-gas critical point for small molecules consisting of up to 12 carbon atoms.

DISCLAIMER

DISCLAIMER

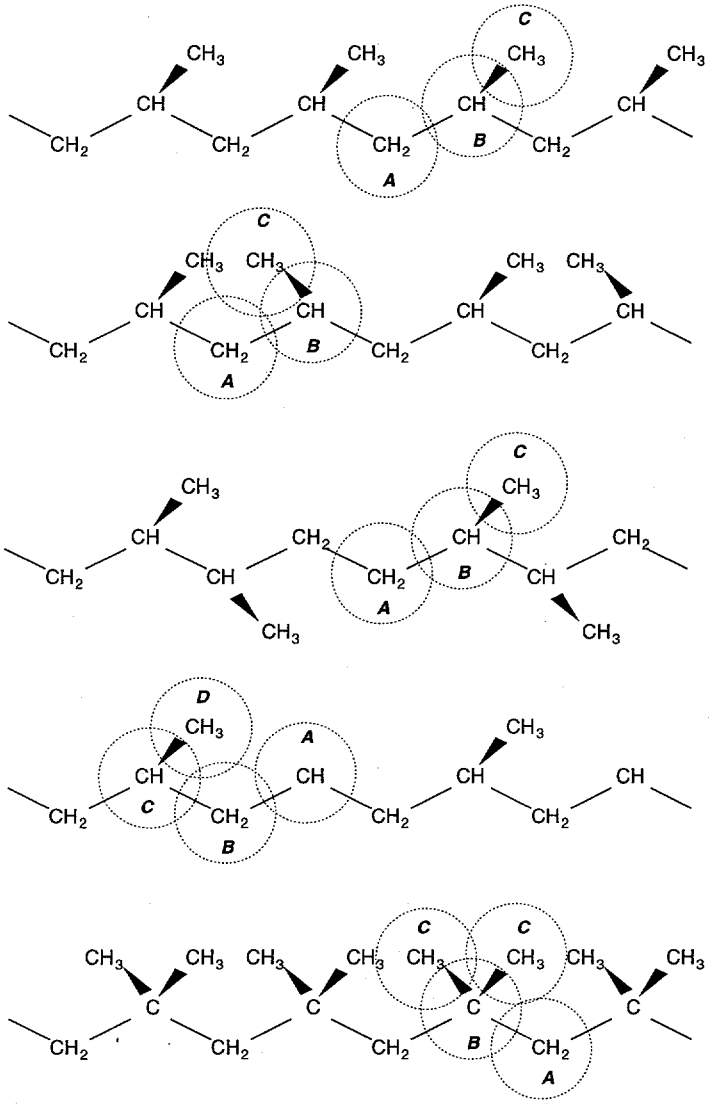

Figure 1: The five polyolefins studied in this work in a graphical representation which corresponds closely to the model we employed: hydrogens together with carbons they are bonded to are modelled by a single spherical site which is indicated by the dotted circles for all sites belonging to a single monomer. We refer to specific sites by the bold italic letters printed in each circle. Only stereo-regular types are studied in this work.

Each carbon with its associated hydrogen atoms is represented by a spherical site. Pairs, inter- and intra-molecular, of sites interact with a Lennard-Jones potential,

$$U(r) = 4\epsilon \left(\left(\frac{\sigma}{r}\right)^{12} - \left(\frac{\sigma}{r}\right)^{6} \right)$$

where the parameters for the various sites are given in table 1. In the MD simulations we used the full potential cut off at a distance of 12Å (including most of the attractive tail) whereas for the PRISM calculations the potential was cut off at its minumum, $r_c = 2^{1/6}\sigma$, and then shifted by ϵ, such that the potential was purely repulsive. The LJ parameters for sites of

different type the standard Berthelot scaling rules were applied,

$$\begin{aligned} \sigma_{ab} &= \tfrac{1}{2}(\sigma_a + \sigma_b) \\ \epsilon_{ab} &= \sqrt{\epsilon_a \cdot \epsilon_b}. \end{aligned}$$

For intra-molecular pairs the LJ potential is only applied, if they are further than three covalent bonds apart.

Covalent bonds between nearest neighbor carbons are modelled by a simple harmonic potential around a finite average distance l_0,

$$V_{bond}(r) = \frac{1}{2} k_{bond} (r - l_0)^2 .$$

The constant k_{bond} is set to the experimental value 900 $\frac{kcal}{mol}$ and the bond length $l_0 = 1.54\text{Å}$ regardless of the number of hydrogens bound to a particular carbon.

To respect the angular geometry of nearest- and next-to-nearest neighbor carbons a harmonic bending potential between three neighboring sites is introduced:

$$V_{bend} = \frac{1}{2} k_{bend} (\Theta - \Theta_0)^2 .$$

The angle θ is defined as the angle in radians between $\mathbf{a}, \mathbf{b}, \mathbf{c}$

$$\cos(\Theta) := \frac{(\mathbf{b} - \mathbf{a}) \cdot (\mathbf{c} - \mathbf{a})}{\|\mathbf{b} - \mathbf{a}\| \, \|\mathbf{c} - \mathbf{a}\|},$$

if $\mathbf{a}, \mathbf{b}, \mathbf{c}$ denote the position vectors for three neighboring sites. The elasticity parameters k_{bend} and the equilibrium angles Θ_0 for the various neighbor triplets are listed in table 2.

Furthermore to incorporate the effect of transitional potential barriers between trans- and gauche-conformations and different population densities of these states a rotational potential for the dihadral angle Φ between nearest neighbor chain-like quadruplets $\mathbf{a}, \mathbf{b}, \mathbf{c}, \mathbf{d}$ is introduced,

$$V_{rot} = \sum_{i=0}^{3} a_i \cos^i(\Phi),$$

where Φ is defined as

$$\cos(\Phi) := \left(\frac{(\mathbf{c} - \mathbf{b}) \times (\mathbf{b} - \mathbf{a})}{\|(\mathbf{c} - \mathbf{b}) \times (\mathbf{b} - \mathbf{a})\|} \right) \cdot \left(\frac{(\mathbf{d} - \mathbf{c}) \times (\mathbf{c} - \mathbf{b})}{\|(\mathbf{d} - \mathbf{c}) \times (\mathbf{c} - \mathbf{b})\|} \right).$$

Table 3 contains the parameters a_i for the various quadruplet combinations of sites. Note, that with our definition of Φ the angle $\Phi = 0°$ corresponds to the *trans* state whereas in [15] (and many other works) *trans* corresponds to $\Phi = 180°$.

In PP and PEP the CH_3 side-groups are not constrained enough by the angle potentials with the backbone chain to remain on one side of the backbone chain in the course of a simulation. In nature such flips of tacticity cannot occur as the H-atom of the CH-group to

which the CH_3-group is attached prevents this. Since in the united atom models the H-atom is not explicitly simulated, we need to introduce a symmetry-breaking potential to incorporate conservation of tacticity into the model. For this purpose we use a so-called improper harmonic torsional potential for the star-like $CH_2 - CH, CH_3 - CH_2$ quadruplets in PP and PEP,

$$V_{impr} = \frac{1}{2} k_{impr} \left(\Psi - \Psi_0\right)^2 ,$$

where Ψ is defined as

$$\cos(\Psi) = \left(\frac{(\mathbf{c}-\mathbf{b}) \times (\mathbf{d}-\mathbf{b})}{\|(\mathbf{c}-\mathbf{b}) \times (\mathbf{d}-\mathbf{b})\|} \right) \cdot \left(\frac{(\mathbf{c}-\mathbf{a}) \times (\mathbf{d}-\mathbf{a})}{\|(\mathbf{c}-\mathbf{a}) \times (\mathbf{d}-\mathbf{a})\|} \right)$$

and $\mathbf{a}, \mathbf{b}, \mathbf{c}, \mathbf{d}$ are the position vectors of the CH and CH_3 and the two backbone CH_2 groups (in the same order). Since ref. [15] does not include these parameters we had to make some reasonable *ad hoc* assumptions: k_{impr} was chosen to be identical to k_{bend} and $\Psi_0 = \pm 30.25°$ depending on the intended tacticity of the chain.

site	ϵ $\left[\frac{kcal}{mol}\right]$	σ [Å]
C	0.00099	6.40
CH	0.0198	4.68
CH_2	0.0912	3.95
CH_3	0.1944	3.73

Table 1: Lennard-Jones interaction parameters for all CH_x groups.

angle triplet	Θ_0	k_{bend} $\left[\frac{kcal}{mol}\right]$
$CH_x - C - CH_y$	109.47	123.75
$CH_x - CH - CH_y$	112.00	123.75
$CH_x - CH_2 - CH_y$	114.00	123.75

Table 2: Bending potential parameters various neighbor triplets.

dihedral quadruplet	a_0	a_1	a_2	a_3
$CH_x - C - CH_2 - CH_y$	0.914913	2.74474	0	-3.65965
$CH_x - CH - CH_2 - CH_y$	0.783911	1.77528	0.443682	-3.50082
$CH_x - CH_2 - CH_2 - CH_y$	0.783911	1.77528	0.443682	-3.50082

Table 3: Torsional potential parameters for various quadruplets. All units are $\frac{kcal}{mol}$.

3 Methodology

3.1 MC/PRISM Calculations

3.1.1 Generalized Ornstein-Zernike-Equation

PRISM theory is an extension to polymers of the reference interaction site (RISM) theory for molecular liquids developed by Chandler and Andersen [16, 17]. Basically it generalizes the

type	N_C	T [K]	ρ [Å^{-3}]	ρ_w [$\frac{g}{cm^3}$]
iPP	36*, 72, 144*, 288	453	0.03282	0.763
sPP	36*, 72, 144, 288	453	0.03282	0.763
hhPP	36*, 72, 144, 288	453	0.03360	0.781
PIB	48*	298	0.03920	0.911
	48*	453	0.03568	0.829
PEP	30*	298	0.03670	0.854

Table 4: Polymer types modelled in this work: iso-tactic poly-propylene (iPP), syndio-tactic poly-propylene (sPP), head-to-head (syndio-tactic) poly-propylene (hhPP), poly-iso-butylene (PIB) and the alternating (iso-tactic) poly-ethylene-propylene copolymer (PEP). Polymers marked with a * have been simulated with MD and PRISM, for others only PRISM calculations were performed. The left-hand side of the table represents simulated chain lenghs in carbons (N_C) with respective temperature (T), carbon number-densities (ρ) and mass densities (ρ_w). ρ_w was taken from experiment for large chain lengths.

Ornstein-Zernike-equation for isotropic atomic liquids [18] to molecular liquids consisting of spherical sites. The radial distribution function matrix, $g_{\alpha\gamma}(r)$, is defined by

$$g_{\alpha\gamma}(\mathbf{r}) = \int \frac{\langle \rho_\alpha(\mathbf{r}')\rho_\gamma(\mathbf{r}-\mathbf{r}')\rangle}{\overline{\rho}_\alpha\overline{\rho}_\gamma} d\mathbf{r}'.$$

In RISM theory the total correlation function $H_{\alpha\gamma}(r) = g_{\alpha\gamma}(r) - 1$ is expanded as as a sum of all possible paths of direct correlations,

$$\begin{aligned} H_{\alpha\gamma}(r) &= \omega_{\alpha\nu}(r) * \overline{\rho}_\nu C_{\nu\mu}(r) * \omega^T_{\mu\gamma}(r) \\ &+ \omega_{\alpha\nu}(r) * \overline{\rho}_\nu C_{\nu..}(r) * \omega_{..,..}(r) * \overline{\rho}_{..} C(r)_{..,\mu} * \omega^T_{\mu\gamma}(r) \\ &+ \text{higher terms.} \end{aligned}$$

The $*$ denotes the standard 3-dimensional convolution integral and the summing convention over equal indices is assumed. This expansion is equivalent to recursing the formula

$$H_{\alpha\gamma}(r) = \omega_{\alpha\nu}(r) * C_{\nu\mu}(r) * \left(\omega^T_{\mu\gamma}(r) + \overline{\rho}_\mu H_{\mu\gamma}(r)\right), \tag{1}$$

which reduces to the Ornstein-Zernike-equation if the liquid consists only of atoms described by a single site (matrices reduce to scalars). $\omega_{\alpha\gamma}(r)$ is the intra-molecular radial distribution function, which basically describes the average shape of a molecule. The function $C_{\alpha\gamma}(r)$ is called the *direct* correlation function and can thought of as an effective medium-induced interaction which acts on sites of type α and γ on two arbitrary molecules. $\overline{\rho}_\alpha$ is the average partial number density for each site-type α. Eq. (1) can be viewed as a definition for $C_{\alpha\gamma}(r)$. Note, that this theory is only approximate since angular correlations between molecules (which are absent in the case for atomic liquids) are not treated explicitly. The intra-molecular distribution function enters this theory as an input field, thus it must be calculated by other means.

Curro and Schweizer [1, 2] applied the RISM theory to polymers by making the additional approximation that different sites along the chain (with equal symmetry and type) can be treated by the same correlation functions. Such a simplification is necessary since the matrices

would otherwise become very large and eventually intractable for big molecules. For ring-polymers the assumption would be correct because of their translational symmetry along the polymer contour; for linear polymers the approximation becomes correct only in the infinite chain limit, though chain-end corrections tend to zero rather quickly.

3.1.2 Closure Relations

Assuming $\omega_{\alpha\gamma}(r)$ is known, the (P)RISM equation (1) contains two unknown functions, $H_{\alpha\gamma}(r)$ and $C_{\alpha\gamma}(r)$, which is useless without additional information. From simulations and experiments on simple liquids one knows that $C_{\alpha\gamma}(r)$ is effectively a short-ranged function and many approximations for $C_{\alpha\gamma}(r)$ have been derived or postulated in the literature [18], most prominently the Percus-Yevick (PY) closure relation,

$$C_{\alpha\gamma}(r) = \left(1 - e^{\beta U_{\alpha\gamma}(r)}\right)\left(H_{\alpha\gamma}(r) + 1\right). \tag{2}$$

Other closures include the hyper-netted chain (HNC) approximation [18] and the Martinov-Sarkisov (MS) relation [19]. For molecular liquids $C_{\alpha\gamma}(r)$ is not necessarily short-ranged, however we will show later how the atomic closure relation (2) may be modified empirically to improve results.

The PY relation is most successful in describing the packing structure in simple hard-core liquids [18]. In general, there is no best generic solution, hence the choice of the approriate closure relation is problem dependent. It has been shown, that the adoption of simple atomic closure relations poses problems for certain applications, e.g. in systems with strong attractions. In these cases more complicated closure relations have to be used. For homo-polymers at melt densities the PY relation has proven to yield results in good agreement to simulations, and we used this relation exclusively throughout this work. Since the PY closure does not work well with attractive tails only the repulsive part of the LJ interactions is used in the PRISM calculations. For dense melts the attractions have very little influence on the packing and may therefore be safely neglected for the structure of the liquid [14]. Thermodynamic quantities, like the compressibility, however are strongly affected by attractive interactions and we will later show how to correct the PRISM results for pure repulsions in a perturbative manner.

The coupled set of non-linear equations (1) and (2) can be solved by the Picard iteration method for the function $\Gamma_{\alpha\gamma}(r) := H_{\alpha\gamma}(r) - C_{\alpha\gamma}(r)$. The reasons why one rather works with Γ instead of C or H directly is that Γ is a continuous function even for hard spheres whereas C and H are not. Also Γ varies over a much broader range of r than each of C (which varies strongly inside the repulsive potential core) and H (which varies strongly outside the core). Equation(1) is actually much easier to solve in Fourier-space because of the convolution integrals whereas the closure relation (2) is easy in real-space since it is local in r . Hence one employs the use of fast Fourier transforms to switch back and forth between r- and k-space representations of the functions.

3.1.3 Self-Consistent Determination of $\omega(r)$

For the case that $\omega_{\alpha\gamma}(r)$ is not known a priori, a hybrid MC/PRISM iterative scheme has been devised to calculate $\omega_{\alpha\gamma}(r)$ in a self-consistent manner. One can generate an initial $\omega^{(0)}_{\alpha\gamma}(r)$ by performing a single chain MC simulation. For chains in a melt one usually expects Flory's

ideality hypthesis to be true and chains should have a random-walk-like self similar structure (for length scales much larger than the peristance length of the chains). A single chain simulation with purely repulsive LJ interactions however will generate chain conformations with the statistics of a self-avoiding random walk, thus $\omega^{(0)}_{\alpha\gamma}(r)$ will be of longer range than the true $\omega_{\alpha\gamma}(r)$. Several approximations have been made in the literature to calculate the effect of the surrounding chains in the medium on the interaction between sites. In general, this is a very complicated task, since the induced interactions are many-body in nature, i.e. the interactions energy induced by the medium should depend on all the positions of all atoms of a single chain simultaneously. So far approximations have been derived only for a *pair-wise* decomposition of this medium-potential. The simplest of these is called the HNC solvation potential, because its derivation borrows from the approximations made in the derivation of the HNC closure relation [20, 21],

$$\beta W_{\alpha\gamma}(r) = -C_{\alpha\nu}(r) * \overline{\rho}_\nu \left(\omega_{\nu\mu}(r) + \overline{\rho}_\nu H_{\nu\mu}(r)\right) * C_{\mu\gamma}(r) \tag{3}$$

or in k-space:

$$\beta \hat{W}_{\alpha\gamma}(k) = -\hat{C}_{\alpha\nu}(k)\overline{\rho}_\nu \hat{S}_{\nu\mu}(k)\hat{C}_{\mu\gamma}(k).$$

Other approximations similar in spirit to the PY and MS approximations have been proposed in the literature [22].

From the $k \to 0$ limit of $\hat{W}_{\alpha\gamma}(k)$ one can deduce that the average value of $W_{\alpha\gamma}(r)$ is negative, which means $W_{\alpha\gamma}(r)$ provides a net attractive force between sites on the same chain and would therefore lead to smaller chain conformations. We can now solve the PRISM equation for $C^{(0)}_{\alpha\gamma}(r)$ and $H^{(0)}_{\alpha\gamma}(r)$ for the initial $\omega^{(0)}_{\alpha\gamma}(r)$ and then use Eqs. (1-3) to calculate a new $W^{(1)}_{\alpha\gamma}(r)$. This new solvation potential can in turn be used to redo the MC calculation of $\omega^{(1)}_{\alpha\gamma}(r)$ and so forth. There is no formal proof that this iterative procedure should actually converge or, equally important, converge to the correct physical result, but it has been checked in previous numerical calculations that the method converges and the results are in very good agreement to simulation results.

It sometimes happens that the convergence is not strong enough and the sequence of $W^{(i)}(r)$ performs small oscillations around the final solution. Then the convergence can usually be forced by mixing the old solution $W^{(i)}$ with the current W to obtain the new guess for $W^{(i+1)}$,

$$W^{(i+1)} = \alpha_w W\left\{W^{(i)}\right\} + (1-\alpha_w)W^{(i)},$$

where α_w is a real number between 0 and 1 ($\alpha_w = 0.3$ for all calculations in this work).

3.1.4 Simulation details

For the MC calculation we employed the standard pivot-algorithm [23] to generate a sequence of chain conformations with the proper statistical distribution. We implemented two types of pivot moves: bending and torsional moves. For the bending moves a random angle-triplet was picked and one arm of the triplet was rotated by a random angle (usually between $\pm 30°$) around the axis perpendicular to the triplet-plane. The acceptance rate for these moves was

usually between 15% and 30%. For the rotational moves a dihedral-quadruplet was chosen at random and the shorter of the two arms was rotated around the center axis by a random angle between $\pm 180°$. The acceptance rate was usually between 7% (PIB) and 30% (PEP). One Monte-Carlo step (MCS) always consisted of one attempted bending and one rotational move.

The pivot algorithm [23] has been shown to efficiently relax all length scales of a (self-avoiding) random-walk chain. The MC autocorrelation time for the end-to-end-distance and radius of gyration of the chain scales proportionally to the length of the chain, unlike local MC algorithms (like kink-jump) where it scales proportionally to the chain length squared. However the time to perform one pivot step is proportional to the chain length squared (because of the non-bonded pair-interactions), so the total amount of computer time scales like the chain length cubed, which is the same for local MC algorithms. For short-ranged potentials and long chains the pivot algorithm can be modified to scale to the first power of the chain length again by using the link-cell method which is commonly used in MD simulations [24]. For PRISM calculations this does not help very much because of the rather long-range nature of the solvation potential. The cut-off for non-bonded interactions has to be chosen rather large, thus the link-cell method speeds up the calculation to some extent, but not as efficiently as with pure LJ-interactions.

For all chains the number of MC steps between calculations of $\omega_{\alpha\gamma}(r)$ was chosen to be about 3 times (4 times for PIB) the number of sites on the chain, which was sufficient for successive calculations of R_e^2 and R_g^2 to be almost completely decorrelated. $\omega(r)$, $H(r)$, $C(r)$ and their Fourier-transformed quantities where discretized on a grid of size G (typically 2048 or 4096) with a lattice spacing of 0.1Å in real-space and $\frac{10\pi}{G}$ Å^{-1} in Fourier-space.

For the initial self-consistent iterations $M = 500$ independent conformations were generated and ω was calculated as an average over these conformations. When the error

$$E_{self} = \left[\frac{2}{N(N+1)G} \sum_{\alpha=1}^{N} \sum_{\gamma=1}^{\alpha} \sum_{n=1}^{G} \left(W_{\alpha\gamma}(r_n) - W_{\alpha\gamma}^{(i)}(r_n) \right)^2 \right]^{\frac{1}{2}}$$

became less than 10^{-2} we generated $M = 5000$ independent conformations for each iteration step thereafter to improve the statistical error. Since at this stage the solvation potential $W_{\alpha\gamma}$ did not change very much we could successfully employ Monte-Carlo reweighting [25] to re-use the conformations generated with an older $W_{\alpha\gamma}$,

$$\langle \omega \rangle \{W_{new}\} = \frac{1}{Z} \sum_{j=1}^{M} \omega^{(j)} \{W_{old}\} \cdot e^{\beta[W_{new}(j) - W_{old}(j)]}$$

with

$$Z = \sum_{j=1}^{M} e^{\beta[W_{new}(j) - W_{old}(j)]}.$$

Using the reweighting technique the number of conformation resamplings was typically less than four. We used the automatic, empirical criterion

$$\min\{Z, 1/Z\} < \frac{M}{4}$$

to determine whether reweighting would still provide acceptable estimates for $\omega_{\alpha\gamma}$ or if we had to restart the chain generation with the Pivot-algorithm.

For the Picard iteration to solve the PRISM equation we used the criterion

$$E_{prism} = \left[\frac{2}{N(N+1)G} \sum_{\alpha=1}^{N} \sum_{\gamma=1}^{\alpha} \sum_{n=1}^{G} \left(\Gamma_{\alpha\gamma}(r_n) - \Gamma_{\alpha\gamma}^{(i)}(r_n) \right)^2 \right]^{\frac{1}{2}} < 10^{-7}$$

for convergence. To insure convergence the iteration was performed using 10% per cent of the new result for $\Gamma_{\alpha\gamma}$ mixed with 90% of the old result for the next iteration.

A full self-consistent MC/PRISM calculation took between 30 minutes (PEP, shortest chains) and 50 hours (PIB, longest chains) of CPU time each on a single Pentium III/450 processor.

3.2 Molecular Dynamics Simulations

Molecular dynamics simulations were only performed for the shortest chain lengths (12 monomer units) except for iPP where an additional simulation of chains with 48 monomers was performed. We used a multiple time step second order symplectical integrator (RESPA) [26] to solve the equations of motion. The temperature was kept constant by employing the standard Nose-Hoover extended ensemble method [27]. Since the bond, bending, torsional and improper potentials have much higher eigen frequencies than the Einstein frequency of caging induced by the non-bonded LJ interactions we could use a $1fs$ timestep for the bond forces, a $2\ fs$ timestep for the angle, torsion and improper forces and a $4\ fs$ timestep for the LJ forces. The Nose-Hoover coupling frequency was chosen to be $0.02fs^{-1}$. At this coupling frequency oscillations in the potential and kinetic energies of the particles were sufficiently suppressed. For all simulations we used a slightly modified version of the LAMMPS code [28]. The simulations were carried out at fixed density (see Tab. 4), corresponding to the experimental density for large chain length to facilitate comparison with X-ray scattering in section 4.5.

The starting configurations were created by the same pivot algorithm that we used in the MC/PRISM calculations. The final solvation potential that was obtained by a self-consistent PRISM calculation was used to generate 100 (60 for iPP with 48 monomers) independent chain conformations which were very close to their equilibrium conformation. These chains were placed randomly inside a cubic box with proper dimension L for a given density, taking no measures to disallow chain overlap. Finally the coordinates were periodically folded into the box. Since the chains were overlapping initially, we used a piecewise linear/cosine-potential

$$U_{push}(r) = \begin{cases} B\left(1 - \pi - \frac{r}{r_c}\right) & \text{for} \quad 0 < r < \frac{r_c}{2} \\ B\left(1 + \cos\left(\pi \frac{r}{r_c}\right)\right) & \text{for} \quad \frac{r_c}{2} < r < r_c \end{cases}$$

with $r_c = 4.0$Å for all LJ interactions independent of the site type. The amplitude, B, was increased linearly from an initial value of $10\frac{kcal}{mol}$ to $70\frac{kcal}{mol}$ within a total simulation time of 1 ps. Thus overlapping chains were pushed apart from each other rapidly, but smoothly. After 1 ps the full LJ-potential could be switched on without problems. This method disturbs the chain conformations only locally, but not on large length scales. The perturbations on small length scales were annealed after a short relaxation period. Note, that the soft U_{push} potential differs inside the core $0 < r < r_c/2$ from the potential that was used in previous studies [29] of

polymer melts. The reason to change to a harder core was that with the pure cosine-potential two sites could on rare occasions get stuck on top of each other with no route of escape since they were caged by surrounding sites. This can happen since the repulsive force is increasing from zero to its maximum for $0 < r < r_c/2$.

After the chains no longer overlapped, we ran each system for a total of 8 ns (25 ns for 48 monomer iPP), of which the first 2 ns (5 ns for 48 monomer iPP) were always discarded in the a posteriori analysis of the data. The coordinates of all particles were written every 200 ps. Typically each of the 8 ns simulations ran about 70 (PEP) to 130 (PIB) hours on 4 Pentium III/450 processors. Comparing this to the PRISM runtimes for the shortest chains this represents a factor of 200 in total CPU time.

4 Results & Discussion

4.1 Inter-molecular Radial Distribution Functions

The most important quantity which PRISM is able to calculate is the site-site radial inter-molecular distribution function $g_{\alpha\gamma}(r)$ which describes the packing structure of the molecules. The knowledge of the site-site interactions and intra- and inter-molecular distribution functions allows one to calculate many important thermodynamic quantities of interest. The emphasis of this work is to test the quality with which PRISM can predict the inter-molecular packing structures for realistic polymer models compared to *exact* results for such models obtained by full scale MD simulations.

In Figs. 2 and 3 we compare PRISM and MD results for all different site combinations for all five polymer models we have tested. It can be seen from these figures that there is good qualitative agreement between PRISM theory and simulation for the polyolefins studied. Examination of the radial distribution functions reveals that the strongest correlations near contact (~4 Å) are the $g_{CC}(r)$ ($g_{DD}(r)$ for PEP) correlations between methyl groups. This is not surprising since the side chain methyl groups are on the outside of the chains and can approach each other readily in the melt. As can be seen in Fig. 2, PRISM theory does quite well in predicting $g_{CC}(r)$ for all PP and PIB, although the $g_{CC}(r)$ are consistently softer than from the simulations and the peak structure appears slightly out-of-phase towards smaller distances compared to the MD results. This finding is consistent with what was found earlier for correlations between methylene groups in polyethylene [14] melts. Similar results can be seen from Fig. 3 for $g_{DD}(r)$. For the polyolefins studied here the methyl side groups tend to shield the backbone sites from approaching each other in the melt. This is clearly seen in Fig. 2 where correlations such as $g_{BB}(r)$ involving backbone sites are almost zero in the 4Å region. It is also evident that PRISM predicts excessively soft correlations between sites (e.g. B sites) that are highly shielded from each other. Fortunately, these buried sites (C or CH groups) do not contribute significantly to the cohesive energy since the LJ attractions for our particular model are much weaker than those of the exposed CH_3 and CH_2 groups (see Tab. 1) and their short-range nature effectively cut off the longer range part of the correlation functions.

In our previous study on polyethylene [14], a considerable improvement in agreement of the $CH_2 - CH_2$ intermolecular correlation function $g(r)$ with the simulation result was obtained by forcing the theoretical compressibility to be correct. This was achieved [14] for a hard core site/site potential by adding a power law attractive tail to the direct correlation function $C(r)$ outside the hard core diameter. The range of $C(r)$ is controlled by the power law exponent and was adjusted to force agreement with the known compressibility. In the case of the multi-site

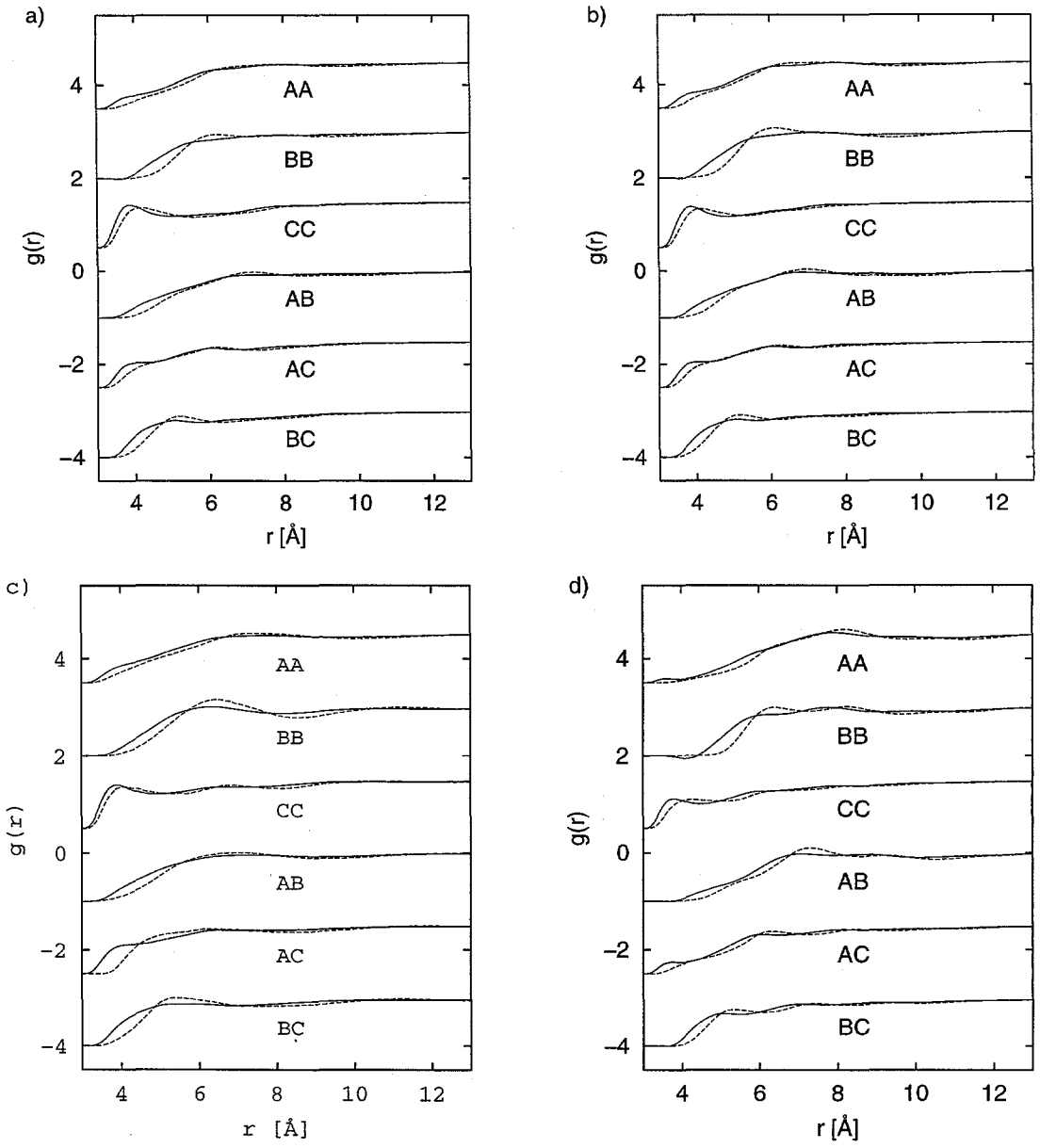

Figure 2: Comparison of $g_{\alpha\gamma}(r)$ for iPP (a), sPP (b), hhPP (c) and PIB (d) from MD and MC/PRISM. All data was obtained from simulations at 453 K. The continuous line represents the PRISM results and the dashed line the MD results.

polyolefins studied here, we have $M(M+1)/2$ independent direct correlation functions (where M is the number of independent sites per monomer) and only one compressibility condition. To investigate this approach in our case we, by analogy with the polyethylene case [14], take the direct correlation functions to obey the closure condition

$$\begin{aligned} g_{\alpha\gamma}(r) &= 0 && \text{for} \quad r < d_{\alpha\gamma} \\ C_{\alpha\gamma}(r) &= C^{(0)}_{\alpha\gamma}(r)\left(\frac{d_{\alpha\gamma}}{r}\right)^{\lambda} && \text{for} \quad r > d_{\alpha\gamma} \end{aligned}$$

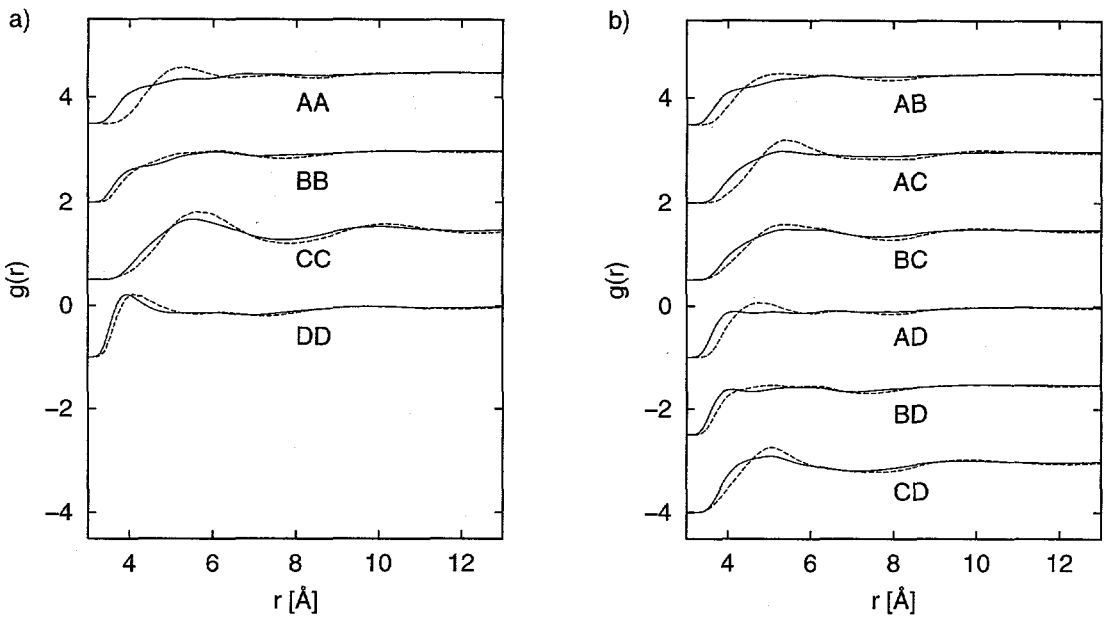

Figure 3: Comparison of $g_{\alpha\gamma}(r)$ for PEP : a) diagonal elements and b) off-diagonal elements. All data was obtained from simulations at 298 K. The continuous line represents the PRISM results and the dashed line the MD results.

where $C^{(0)}_{\alpha\gamma}(r)$ is the direct correlation function satisfying the PY hard core closure inside the hard core, and $d_{\alpha\gamma}$ is the corresponding hard core diameter obtained by using the Barker-Henderson or WCA mapping from a continuous Lennard-Jones potential [18]. For simplicity, we take the range parameter λ to be the same for all of the site-site direct correlation functions. In this way we have only a single parameter, λ, adjusted to 9.6, to adjust to force agreement with the compressibility.

We have carried out this procedure for the case of iPP and the results are shown in Fig. 4. It can be seen that there is some improvement in the agreement between theory and simulation, especially for the peak positions of the correlation functions of the exposed C-sites which are matched up with those of the MD simulation. Of course, the improvement is not as dramatic as in the case of polyethylene where we had only one direct correlation function, since λ is undoubtedly different for each of the $C_{\alpha\gamma}(r)$ functions. But without additional information from simulation (or experiment) a more general ansatz for the tail correction is unfeasable. This is a consequence of the fact that the total structure factor $S_{\alpha\gamma}(0)$ and $\omega_{\alpha\gamma}(0)$ are singular matrices.

An alternative way to correct the PRISM results would be to increase the effective LJ diameters, σ, by some amount, which would increase the effective density and thereby counter PRISM's tendency to predict too high compressibilities. Of course, this would also have implications on the self-consistent calculation of $\omega(r)$.

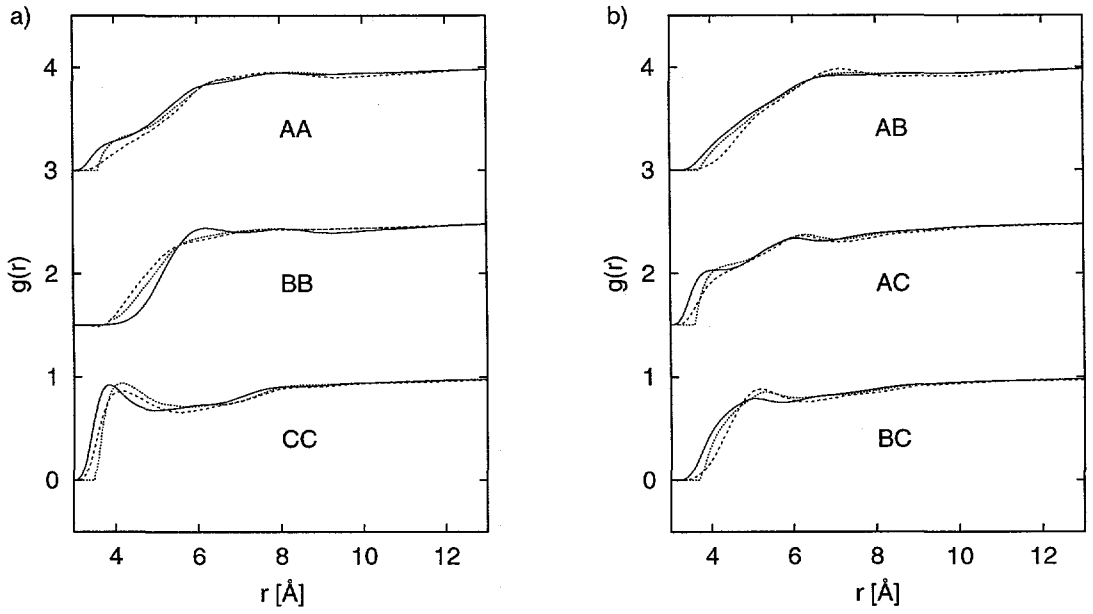

Figure 4: Comparison of $g_{\alpha\gamma}(r)$ for MD (dashed), self-consistent PRISM (continuous) and tail-corrected PRISM (dotted) for iPP: a) diagonal and b) off-diagonal elements.

4.2 Cohesive Energy Densities

The cohesive energy density Π and solubility parameter δ are defined according to the relations

$$\Pi = 2\pi \sum_{\alpha\gamma} \int_0^\infty \rho_\alpha \rho_\gamma U_{\alpha\gamma} r^2 dr \tag{4}$$

and

$$\delta = \sqrt{\Pi}. \tag{5}$$

The cohesive energy densities were calculated from Eq. (5) and the radial distribution functions shown in Figs. 2 and 3 and are given in Tab. 5 from both PRISM theory and from the MD simulations. Not surprisingly, the PRISM values are consistently lower than the corresponding MD simulations due to the fact that PRISM theory overpredicts the amount of overlapping of intermolecular sites. Nevertheless there is good agreement between theory and simulation for the relative values of the solubility parameters among the various polyolefins. If we use the compressibility-corrected $g_{\alpha\gamma}(r)$ the PRISM prediction for the cohesive energy densities increases and is in fact higher than the simulation results, though the overall difference to MD is diminished significantly.

For comparison we also show Π from previous MD simulations on short chains for a different polyolefin model [30] and the related internal pressure,

$$\Pi^* = \left(\frac{\partial U}{\partial V}\right)_{T,N},$$

from experimental measurements for long chain lengths. It was shown in [30] that Π and Π^* show very similar behavior, with Π being consistently smaller than Π^*. Π^* from MD

simulations agreed well with experimental data once Π^* was extrapolated for infinite chain lengths. The model used in this work gives slightly smaller cohesive energies than that from [30] except for PIB which is larger. The results for PEP are not really comparable since the temperatures at which they were calculated differ significantly.

type	T $[K]$	Π_{PRISM}	Π_{MD}	$\Pi_{MD-2}(423K)$	$\Pi^*_{exp}(440K)$
PE	448	161 (199)	187	232	312
iPP	453	131 (166)	155	174	252
sPP	453	136	150	183	
hhPP	453	145	176	198	278
PIB	453	171	199	183	302
PIB	298	126	155		
PEP	298	210	229	207	280

Table 5: Cohesive energy density Π for the shortest simulated chains (24 backbone carbons) and Internal Pressure Π^* for long chain experimental systems. Π_{MD-2} was taken from [30] and Π^*_{exp} from [31]. Numbers in parenthesis are calculated from compressibility-corrected PRISM calculations. All units in MPa.

4.3 Single-Chain Statistics

From Fig. 5 and Tab. 6 it can be seen that there is good agreement between the average single chain dimensions between PRISM theory and MD simulation for short chains, as measured by the mean square end-to-end distance $\langle R_e^2 \rangle$, radius of gyration $\langle R_g^2 \rangle$, and characteristic ratio C_N, with the exceptions of PIB and PEP. This is not surprising since both the theory, through the single chain Monte Carlo simulation, and the full MD simulations treat the single chain problem with almost exactly the same potential parameters in the zero density limit. The only difference is the fixed bond length used in the MC calculations and the harmonic potential used for MD. At high density, it is likely that the solvation potential in Eq. (3) does not appreciably affect the average single chain dimensions on short length scales due to the inherent chain stiffness imparted by the bond angle and rotational constraints. This is confirmed in Fig. 6 where it can be seen that there is essentially exact agreement between theory and MD simulation for the single chain structure factor for higher k -vectors. A more detailed comparison at short length scales will be given in the next section.

For the three polypropylenes under investigation, we also performed self-consistent PRISM calculations as a function of chain length in the range of 12 - 96 monomeric units. For longer chain lengths of the iPP and hhPP studied with PRISM theory, the characteristic ratios can be seen from Tab. 6 to be significantly larger than the experimental values measured by SANS experiments on the melts of long chain polymers, e.g. iPP: $C_\infty = 6.2$ [32]. These differences are mostly due to the small chain lengths studied in this work. Furthermore it can be noticed in Fig. 5 that the scaling of $\langle R_e^2 \rangle$ and $\langle R_g^2 \rangle$ with chain length is higher than $\propto N$ and the ratio R_e^2/R_g^2 is quite a bit larger than the value of 6 expected for a Gaussian coil out to chain lengths of 96 monomers. The correct ideal scaling should be attained for longer chain melts; for PE the Gaussian limit is reached only for chain lengths of about 400 carbons and higher [33]. In order to introduce more molecular realism in the PRISM calculation, one could scale the approximate solvation potential in Eq. (3) by a constant in order to force self-consistent PRISM theory to produce the correct characteristic ratio if the experimental value is known.

A more rigorous attempt to the correct the solvation potential would involve higher order correlation functions and thus a multi-body solvation potential.

type	T [K]	N_M	R_e^2	R_g^2	C_N	R_e^2/R_g^2	R_e^2	R_g^2	C_N	R_e^2/R_g^2
iPP	453	12	276(3)	38.2(2)	5.06	7.23	259(4)	36.7(2)	4.75	7.06
		24	697(9)	97.7(8)	6.25	7.13				
		48	1570(30)	235(3)	6.97	6.68	1230(50)	196(5)	5.46	6.3
		96	3500(60)	540(6)	7.73	6.48				
sPP	453	12	399(4)	49.2(3)	7.31	8.11	384(4)	47.8(2)	7.04	8.03
		24	1007(15)	134(1)	9.03	7.51				
		48	2386(45)	344(4)	10.6	6.94				
		96	5270(70)	791(8)	11.6	6.66				
hhPP	453	12	383(4)	48.3(3)	7.02	7.93	389(3)	48.2(2)	7.13	8.07
		24	996(10)	134(1)	8.94	7.43				
		48	2363(35)	339(3)	10.5	6.97				
		96	5200(50)	800(6)	11.5	6.50				
PIB	298	12	266(5)	41.0(4)	4.88	6.49	309(4)	43.1(2)	5.66	7.17
	453	12	279(4)	42.0(3)	5.11	6.64	259(2)	41.1(1)	4.74	6.30
PEP	298	6	315(2)	42.3(2)	5.77	7.45	350(3)	46.6(2)	6.42	7.51

Table 6: Single chain statistics and solubility parameters for all systems simulated by PRISM (left half of the table) and MD (right half). Units for lengths are Å.

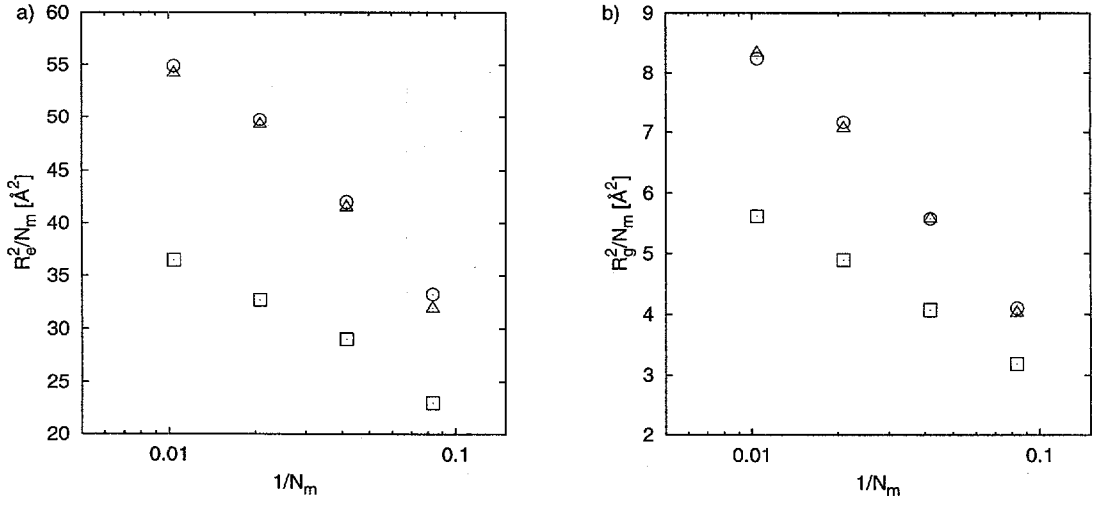

Figure 5: a) Squared end-to-end distance $\langle R_e^2 \rangle$ and b) radius of gyration squared $\langle R_g^2 \rangle$ divided by the number of monomers N_m vs. $1/N_m$ for various types of poly-propylene: iPP (□), sPP (○) and hhPP (△).

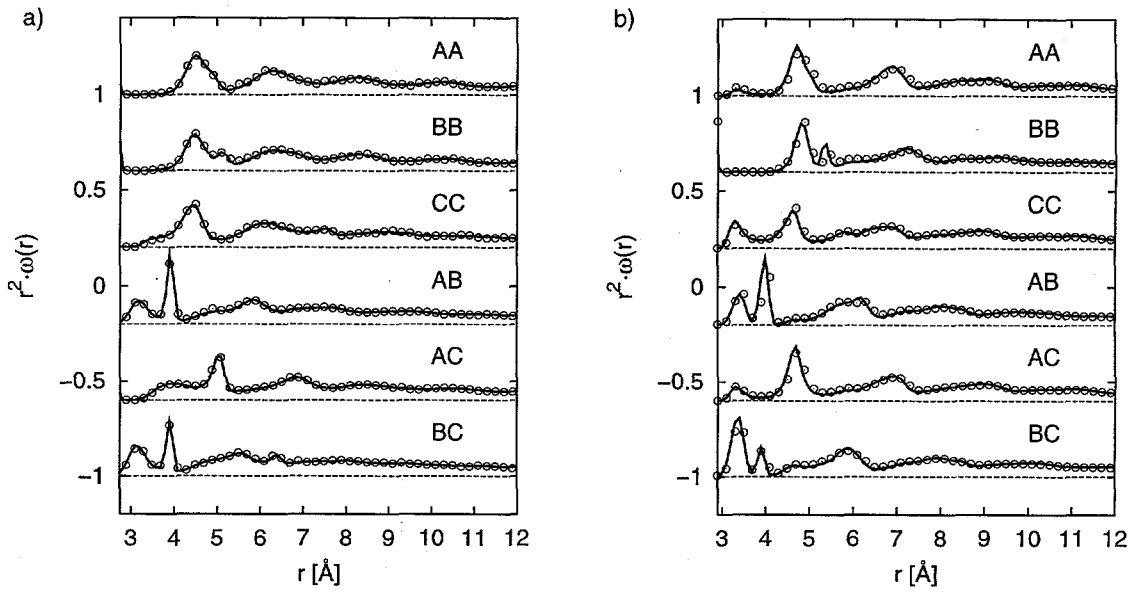

Figure 6: Intra-molecular distribution function $\omega(r)$ weighted by r^2 for iPP (a) and PIB (b) from MD (o) and PRISM (continuous line). The sharp, high peaks from the 1-2 and 1-3 nearest neighbors have been removed and, for clarity, only every other data point of the MD analysis is shown.

4.4 Bending and Dihedral Angle Distributions

While the agreement of PRISM vs. MD is very good in the single chain statistics for all the PP models, some notable disagreement can be found for PIB. Also the extrapolated stiffness for infinitely long chains for all the chains is consistently overpredicted vs. experimental values. The are two possible explanations reasons for the discrepancy: The model is not accurate enough to reproduce the correct chain stiffness or the HNC approximation for the solvation potential is too weakly attractive. To address this question we performed a MD simulation for iPP with 48 monomer units to see whether the MD results predict a significantly lower chain stiffness. From Tab. 6 it can be seen that the MD result for the 48 monomer chain gives considerably smaller values for R_e^2, R_g^2 and C_N. The chain is already much closer to being Gaussian than predicted by PRISM theory as can be seen from the ratio R_e^2/R_g^2. Hence we must conclude that the solvation potential is too weakly attractive to collapse the chain to a Gaussian coil. From Tab. 6 we can also see that PRISM predicts an expansion of the radius of gyration and end-to-end-distance of the chains for PIB with temperature whereas MD (and experiment) predict a negative temperature expansion coefficient.

In order to better our understanding of the effects of the solvation potential or interchain non-bonded interactions on the internal structure of the chains we looked more closely at bending and dihedral angle distributions for iPP and PIB. These are displayed in Figs. 7 and 8. In addition to the usual fixed bond self-consistent PRISM calculation and the flexible bond MD simulation we performed two additional calculations. In one of them we did a self-consistent PRISM calculation with flexible bonds (as in the MD simulation) in order to test the influence of bond flexibility. In the other calculation we also used the flexible bonds and did a non-self-consistent PRISM calculation where solvation potential was set to zero.

The latter provides us with information about the overall effect of the solvation potential. For iPP (Fig. 7) the distributions for an isolated chain are hardly affected by either non-bonded interactions or solvation potentials, whereas for PIB (Fig. 8) some influence on the dihedral angle distribution exists. The latter is a consequence of the fact the the asymmetry of the dihedral angle position is induced by the 1-5 interactions between CH_3 sites alone (the sum of all contributing dihedral angle potentials for a backbone bond is symmetricwith respect to *gauche* and *trans* positions), whereas in iPP its influence is considerably weaker and, to a large degree, induced by the dihedral potentials. Therefore the solvation potential does change the dihedral angle distributions for PIB as can be readily seen by comparing the flexible bond self-consistent PRISM with the non-self-consistent one in Fig. 8. From the same figure it seems the flexible bond PRISM calculation captures the influence of the melt on the distribution better than the PRISM calculation with fixed bonds. This is a possible origin for the misprediction of the thermal expansion for PIB in Tab. 6; indeed the flexible bond PRISM calculation gives a $R_e^2(453K) = 366(7)$ and $R_e^2(298K) = 322(5)$ which predicts the correct temperature expansion, but the overall chain expansion is too large. The latter is a consequence of the result that the flexible bond PRISM calculation also predicts the solvation potential to be much weaker than in the case with fixed bonds.

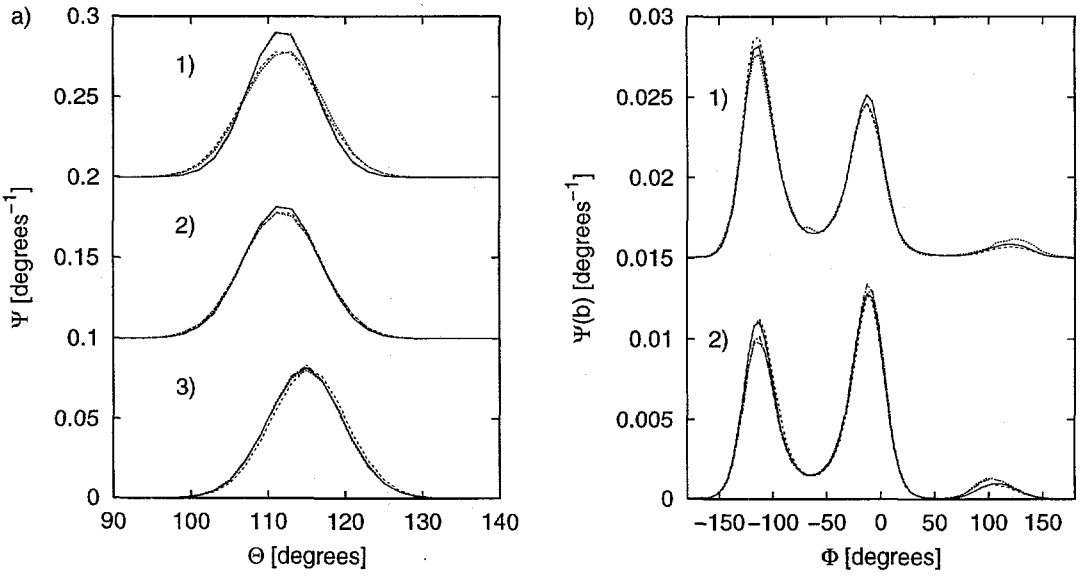

Figure 7: Bending angle (a) and dihedral angle (b) distributions of iPP for MD (continuous line), flexible bonds single-chain MC (dashed), flexible bonds self-consistent PRISM (dotted) and fixed bond self-consistent PRISM (dash-dotted). a.1.: ABC-angle, a.2.: BAB-angle, a.3.: ABA-angle, b.1.: BABA-dihedral, b.2.: CBAB-dihedral.

4.5 Comparison with X-ray Scattering

We have also computed the partial structure factors from PRISM theory and MD simulation from the definition [5, 18]

$$\widehat{S}(k)_{\alpha\gamma} = \rho_\alpha \widehat{\omega}(k)_{\alpha\gamma} + \rho_\alpha \rho_\gamma \widehat{h}(k)_{\alpha\gamma}$$

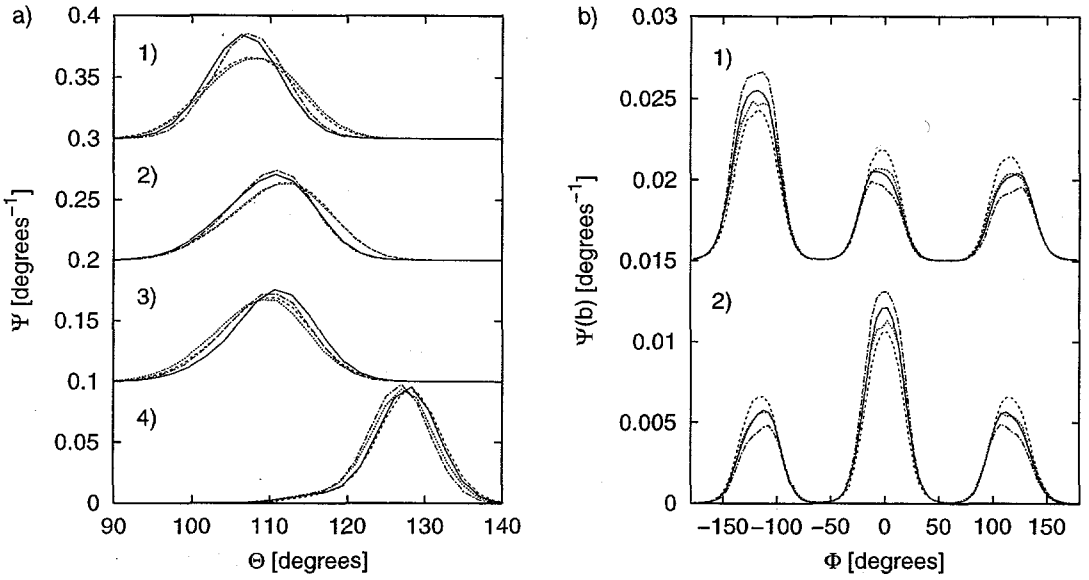

Figure 8: Bending angle (a) and dihedral angle (b) distributions of PIB for MD (continuous line), flexible bonds single-chain MC (dashed), flexible bonds self-consistent PRISM (dotted) and fixed bond self-consistent PRISM (dash-dotted). a.1.: CBC-angle, a.2.: ABC-angle, a.3.: ABA-angle, a.4.: BAB-angle, b.1.: BABA-dihedral, b.2.: CBAB-dihedral.

using the intramolecular structure factors and the Fourier transform of the individual intermolecular correlation functions. The partial structure factors can then be used to make contact with experimental x-ray scattering intensity $I(k)$ through the relation

$$I(K) = \sum_{\alpha\gamma} b_\alpha(k) b_\gamma(k) \widehat{S}_{\alpha\gamma}(k)$$

where the $b_\alpha(k)$ functions are the scattering form factors for the various site types. The scattering data are typically expressed on a per site basis $H(k)$ defined as [34]

$$\widehat{H}(k) = \frac{N_s \left(I(k) - S_s(k)\right)}{\left(\sum_\alpha n_\alpha b_\alpha(k)\right)^2}$$

where n_α and N_s are the number of sites of type α and total number of sites per monomer respectively and $S_s(k) = \sum_\alpha b_\alpha^2(k)$ is the self scattering contribution (then $\widehat{H}(k) \to 0$ for $k \to \infty$).

The PRISM and MD results for the shortest chains along with the experimental scattering functions are shown in Fig. 9. Inspection of Fig. 9 indicates good agreement between theory and simulation for $\widehat{H}(k)$. As expected, there is exact agreement between PRISM theory and MD simulations in the high wave vector regime since scattering in this region essentially probes the single chain structure of the macromolecules. The main peak at $\approx 1\text{Å}^{-1}$ contains information about both inter and intramolecular structure. It can be seen that PRISM theory predicts the height of this main peak to be somewhat lower than from the MD calculations. This is a consequence of the larger theoretical compressibility κ_T caused by the excessive site overlap of sites predicted by the theory.

From Fig. 9 it can be seen that the zero wave vector structure factors from theory and simulation seem to be in close agreement. This would imply, therefore, that the compressibilities would also be in agreement since $S(0) = \rho^2 k_B T \kappa_T$. It should be pointed out, however, that the PRISM theory employed a purely repulsive shifted Lennard-Jones potential, whereas in the in MD simulations the entire Lennard-Jones potential, including the attractive branch, was used. Attractions are known not to be important in determining the short-range structure or pair correlation functions of polymer melts which are dominated by the purely repulsive part of the potential. Attractions, however, can have a very significant effect on thermodynamic properties such as the compressibility. Hence one would expect differences between theory and MD simulation for the zero wave vector structure factor. In fact inclusion of the effect of attractions through perturbation theory would significantly increase the theoretical structure factor in the vicinity of $k = 0$ shown in Fig. 9.

The experimental structure factor obtained from wide angle x-ray scattering experiments [6, 34, 35] are also shown in Fig. 9. Overall agreement is quite good considering the fact that PRISM and MD simulation results are for short chains and experiments are for long chains. Part of this due to the fact that the monomer density is the same for all three. The differences in the structure factor at high wave vectors between the experiment and both theory and simulation reflect the fact that the local bond lengths, bond angles, and rotational potentials used in the computations do not completely model the reality of the actual polyolefin chains studied experimentally. It is interesting to note that the MD simulations are in reasonably good agreement with experiment for the main peak in the structure factor for all the polyolefins except hhPP. The lesser agreement of our results for hhPP could be consequence of the fact that the experimental systems are atactic whereas we have chosen a syndiotactic order in order to avoid the necessary quenched average over the different tacticities. Also little is known about the ratio of iso- and syndiotactic states in hhPP.

To check the influence of chain length on the structure factor we simulated a 48 monomer iPP chain and compared $H(k)$ for both 12 and 48 monomers in Fig. 10a. For comparison results from the PRISM calculation are shown in in Fig. 10b. While the high wave vector regime is not influenced at all, the compressibility for the simulated system turns out to be about 10% larger for the longer chains and the height of the first peak is also about 5% larger and slightly shifted to smaller k-values. The higher compressibility can be understood as a consequence of the effectively smaller density of the long chain system because there are less chain ends per total number of monomers. Overall the differences are fairly small but they should be taken into consideration as systematic correction for the comparison to experimental data in Fig. 9.

Given that the PRISM and MD results for $H(k)$ agree quite favorably and PRISM is a computationally more efficient than MD, we believe that PRISM is an excellent method to distinguish between different potentials. This is particularly important for PIB, where most potential sets give fairly poor results for $H(k)$. To demonstrate this point we did a self-consistent PRISM calculation for the PIB model presented in [30]. From Fig. 11 we can see that the present model agrees somewhat better to the experimental data in the low k region, i.e. the packing is better described mainly as consequence of the different LJ interactions. On the other hand the model from [30] is slightly better in the high k region. The latter is largely due to a too small BAB-angle in the model used in this work. It can be seen from Fig. 8 a) that the BAB-angle is stretched far above the average angle of 114° and closer to 122° from the model in [30] as consequence of the strong repulsion of neighboring CH_3 groups. The good agreement to experimental $H(k)$ data obtained in [5] was using essentially the same model as

in [30] however the 1-5 interactions were tuned to optimize the agreement with experimental $H(k)$. In the present model no tuning was done. Clearly the 1-5 interaction between the CH_3 sites in PIB is a crucial parameter for obtaining good agreement with experimental data. For the other polyolefins, the two potential sets give comparable results [35].

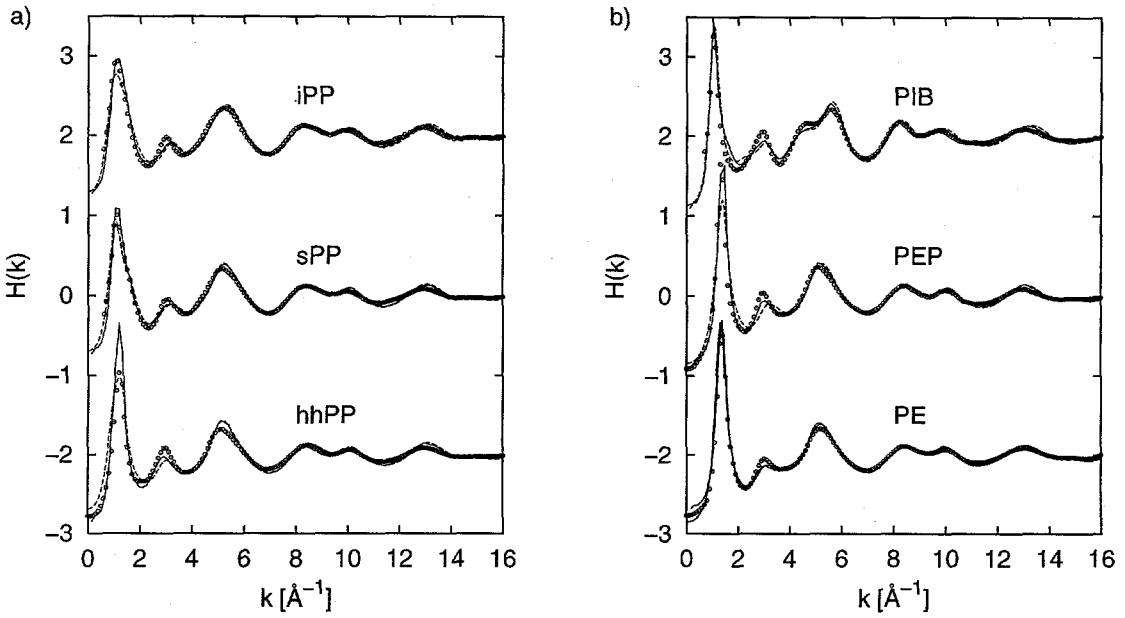

Figure 9: Total structure function measured by X-ray scattering [6, 34](∘) compared to the MC/PRISM (dashed) and MD (continuous) result for the shortest chains. All PP and PIB results are at $453K$, PEP at $298K$ and PE at $448K$ (taken from [14]). PRISM results have not been corrected for LJ attractions and bond lengths were kept constant.

5 Conclusion and Outlook

In this investigation we have shown that self-consistent PRISM theory gives good agreement with exact simulations of polyolefin melts. The agreement, however, falls short of being quantitative. As in our earlier study on polyethylene, the shortcomings of the theory are probably due to the inability of RISM theory to treat sites that are significantly overlapped. Another contributing factor could also be the presence of local nematic ordering between chains. For polyethylene it was demonstrated that local nematic ordering increases as bond angle constraints and torsional potentials are introduced into the model. PRISM theory is incapable of accounting for these angular correlation effects.

Clearly the solvation potential used in this work is an insufficient approximation to obtain the correct scaling for the radius of gyration of long chains. One may artificially fix this behavior by introducing a variable prefactor in front of Eq. (3) in order to get the correct scaling [5, 6] however this diminishes the predictive power of the theory. For future applications better approximations would be desirable. Nontheless the overall quality of agreement in the total structure factor with MD simulations makes self-consistent PRISM a valuable tool for distinguishing potential differences quickly and may be used for tuning them.

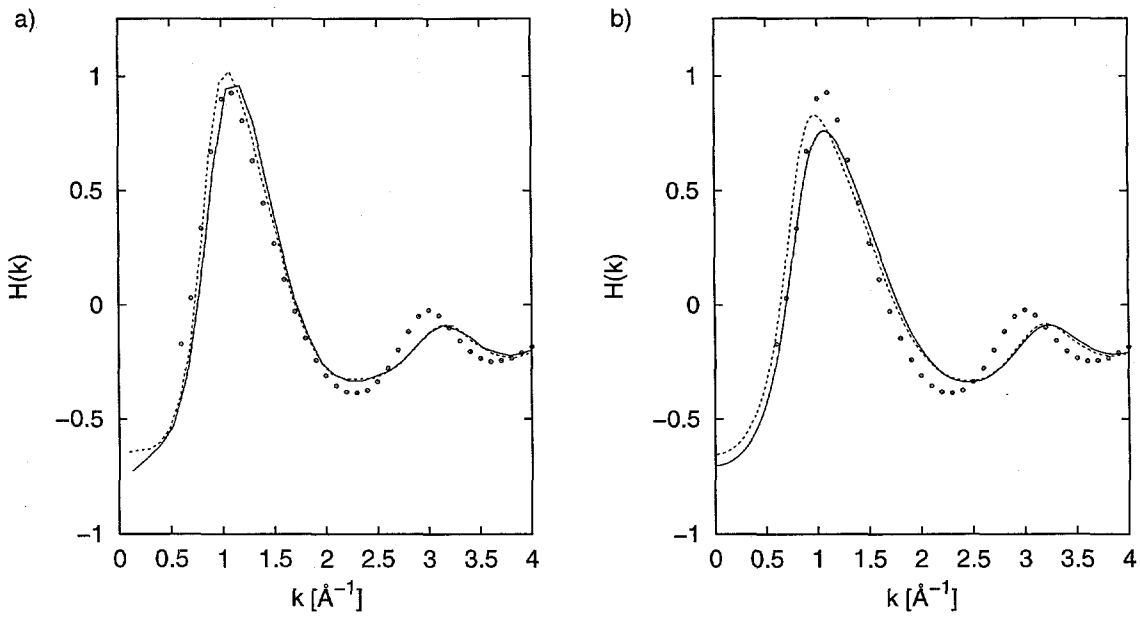

Figure 10: Comparison of total structure factor of iPP for 12 monomers (continuous) and 48 monomers (dashed) from MD calculations (a) and (fixed bond length) self-consistent PRISM (b) compared to X-ray scattering (o).

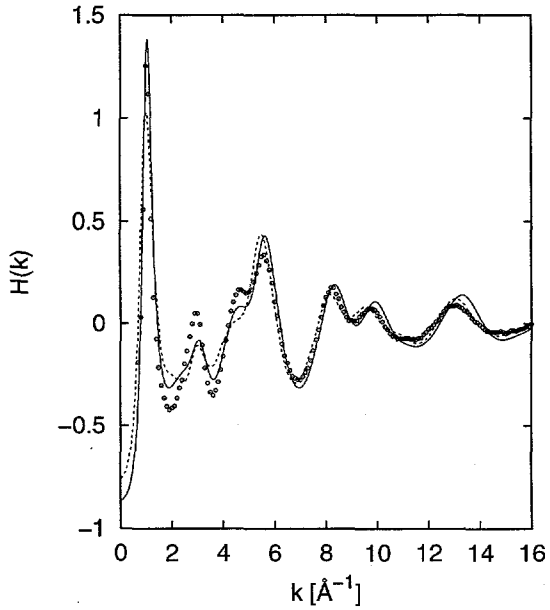

Figure 11: Total structure function for two different models of PIB calculated by (fixed bond length) self-consistent PRISM - ref. [15] (continuous) and ref. [30] (dashed) - compared to experimental data (o).

In self-consistent PRISM theory we treat the single chain part of the problem exactly through a single chain Monte Carlo simulation. The many chain effects are approximately

accounted for in the solvation potential. If one is interested in obtaining a more quantitative theory, one could treat the problem exactly at the two-chain level as suggested in [36]. In this approach one does a two-chain Monte Carlo simulation to obtain the various $g_{\alpha\gamma}(r)$. The remaining chains in the melt or blend are mimicked using the same solvation potential employed here between intra and intermolecular sites of the two chains during the two-chain simulation. Such calculations are numerically feasible by taking advantage of reweighting techniques so that the Monte Carlo simulation does not have to be performed for each iteration of the self-consistent computation of $g_{\alpha\gamma}(r)$. This work will be the subject of a future investigation.

Acknowledgements The authors thank A. Habenschuss for providing us with the refined X-ray scattering data on the polyolefins shown in Figs. 9 and 10. Sandia is a multiprogram laboratory operated by Sandia Corporation, a Lockheed Martin Company, for the United States Department of Energy under Contract DE-AC04-94AL85000.

References

[1] K. S. Schweizer and J. G. Curro, Adv. Polym. Sci. **116**, 319 (1994).

[2] K. S. Schweizer and J. G. Curro, Adv. Chem. Phys. **98**, 1 (1997).

[3] K. G. Honnell, J. D. McCoy, J. G. Curro, K. S. Schweizer, A. Narten, and A. Habenschuss, J. Chem. Phys. **94**, 4659 (1991).

[4] A. Narten, A. Habenschuss, K. G. Honnell, J. D. McCoy, J. G. Curro, and K. S. Schweizer, Faraday Trans. **88**, 1791 (1992).

[5] J. G. Curro, J. D. Weinhold, J. J. Rajasekaran, A. Habenschuss, J. D. Londono, and J. D. Joneycutt, Macromolecules **30**, 6264 (1997).

[6] J. D. Weinhold, J. G. Curro, A. Habenschuss, and J. D. Londono, Macromolecules **32**, 7276 (1999).

[7] J. G. Curro, K. S. Schweizer, G. S. Grest, and K. Kremer, J. Chem. Phys. **89**, 1357 (1989).

[8] A. Yethiraj, C. K. Hall, and K. G. Honnell, J. Chem. Phys. **93**, 4453 (1990).

[9] A. Yethiraj and C. K. Hall, J. Chem. Phys. **96**, 797 (1992).

[10] C. S. Stevenson, J. D. McCoy, S. J. Plimpton, and J. G. Curro, J. Chem. Phys. **103**, 1200 (1995).

[11] C. S. Stevenson, J. G. Curro, J. D. McCoy, and S. J. Plimpton, J. Chem. Phys. **103**, 1208 (1995).

[12] A. Tillman, D. R. Rottach, J. D. McCoy, S. J. Plimpton, and J. G. Curro, J. Chem. Phys. **107**, 4024 (1997).

[13] A. Tillman, D. R. Rottach, J. D. McCoy, S. J. Plimpton, and J. G. Curro, J. Chem. Phys. **109**, 806 (1998).

[14] J. G. Curro, E. B. Webb, G. S. Grest, J. D. Weinhold, M. Pütz, and J. D. McCoy, J. Chem. Phys. **111**, 9073 (1999).

[15] M. Martin and I. Siepmann, J. Phys. Chem. B. **103**, 4508 (1999).

[16] D. Chandler and H. C. Andersen, J. Chem. Phys. **51**, 1930 (1972).

[17] D. Chandler, in *Studies in Statistical Mechanics*, edited by E. W. Montroll and J. L. Lebowitz (North-Holland, Amsterdam, 1982).

[18] J.-P. Hansen and I. R. McDonald, *Theory of Simple Liquids* (Academic Press, London, 1986).

[19] G. A. Martinov and G. N. Sarkisov, Mol. Phys. **49**, 1495 (1983).

[20] D. Chandler, Y. Singh, and D. M. Richardson, J. Chem. Phys. **91**, 1975 (1984).

[21] A. L. Nichols, D. Chandler, Y. Singh, and D. M. Richardson, J. Chem. Phys. **81**, 5109 (1984).

[22] C. J. Grayce and K. S. Schweizer, J. Chem. Phys. **100**, 6846 (1994).

[23] N. Madras and A. D. Sokal, J. Stat. Phys. **50**, 109 (1988).

[24] M. P. Allen and D. J. Tildesley, *Computer Simulation of Liquids* (Clarendon Press, Oxford, 1987).

[25] R. H. Swendsen and R. H. Ferrenberg, Phys. Rev. Lett. **61**, 2635 (1988).

[26] M. Tuckerman, B. J. Berne, and G. J. Martyna, J. Chem. Phys. **97**, 1990 (1992).

[27] S. Nose, Mol. Phys. **52**, 255 (1984).

[28] S. Plimpton, J. Comp. Phys. **117**, 1 (1995).

[29] K. Kremer and G. S. Grest, J. Chem. Phys. **92**, 5057 (1990).

[30] J. Maranas, M. Mondello, G. S. Grest, S. K. Kumar, P. D. Debenedetti, and W. W. Graessley, Macromolecules **31**, 6991 (1998).

[31] R. Krishnamoorti, W. W. Graessley, G. T. Dee, D. J. Walsh, L. J. Fetters, and D. J. Lohse, Macromolecules **29**, 367 (1996).

[32] D. G. H. Ballard, P. Cheshire, G. W. Longmann, and A. Schelter, Polymer **19**, 379 (1978).

[33] M. Mondello, G. S. Grest, E. B. Webb III, and P. Peczak, J. Chem. Phys. **109**, 768 (1998).

[34] J. D. Londono, A. Habenschuss, J. G. Curro, and J. J. Rajasekaran, J. Polym. Sci. B Poly. Phys. **34**, 3055 (1996).

[35] J. D. Londono, J. K. Maranas, M. Mondello, A. Habenschuss, G. S. Grest, P. G. Debenedetti, W. W. Graessley, and S. K. Kumar, J. Polym. Sci. B Poly. Phys. **36**, 3001 (1998).

[36] J. P. Donley, J. G. Curro, and J. D. McCoy, J. Chem. Phys. **101**, 3205 (1994).